Engineering Structures 327 (2025) 119654

Contents lists available at ScienceDirect

Engineering Structures

journal homepage: www.elsevier.com/locate/engstruct

Shear strength model for UHPC members incorporating fiber orientation and cross-sectional shape effects: Model formulation and database evaluation

Amjad Diab [a,*], Anca Ferche [b]

[a] The University of Texas, Austin
[b] Architectural & Environmental Engineering, 301 E. Dean Keeton St., Austin, TX 78712-C1748

ARTICLE INFO

Keywords:
UHPC
Shear strength
Database
Fiber orientation
Cross-sectional shape effect

ABSTRACT

A model for calculating the shear strength of ultra-high performance concrete (UHPC) members is presented. The model employs a hybrid approach that integrates theoretical formulations based on the Modified Compression Field Theory with elements derived from experimental observations and analytical studies to account for the implications of cross-sectional shape effect and the fiber orientation. Additionally, a new expression for determining the angle of the diagonal compressive stresses in UHPC members is introduced, developed from compatibility conditions. An extended database was compiled from the literature, containing 534 experimental results of shear-critical UHPC beams, covering a wide range of test parameters from 51 distinct studies. The accuracy of the proposed model was verified against this database. A reasonably good performance was achieved in calculating the shear strength of UHPC beams with a coefficient of determination of 0.95, an average ratio for the experimental-to-calculated strength of 1.05, and a coefficient of variation of 0.27.

1. Introduction

The utilization of ultra-high performance concrete (UHPC) holds potential to revolutionize infrastructure design and construction and reduce maintenance costs [1,2]. The superior mechanical properties and durability of UHPC facilitate the development of innovative, sustainable structural members with thinner sections and reduced amount of conventional steel reinforcement, compared to conventional concrete members [3–7]. A major barrier to the broader application of UHPC members lies in the development of reliable design guidelines, with flexural and shear strength models being of primary importance. While the flexural mechanisms in UHPC members are relatively well-understood and the recently developed flexural strength models give accurate results [8–10], the shear-carrying mechanisms have proven to be more challenging to characterize. Table 1 and Fig. 1 summarize four existing shear strength models and their performance calculating the nominal shear strength of specimens reported in the literature, including a total of 212 beams. References and details of the specimens included in this comparison are provided in Table 2 in the following section. These models include the fib Model Code [11], Association Française de Génie Civil (AFGC) code [12], PCI design guidelines [13], and the AASHTO guide specifications [14], respectively. The database compiled for this assessment includes prestressed and non-prestressed specimens with varying cross-sectional shapes, described in detail in the following sections. To objectively evaluate the models' ability to predict shear strength, specimens with conventional transverse reinforcement were excluded, focusing on cases where UHPC material serves as the primary shear-resisting mechanism. The comparison was conducted following the expressions summarized in Table 1, without applying safety factors, to assess these models' accuracy in calculating the nominal strength compared to experimentally-measured values. As shown in Fig. 1, the accuracy of the existing models varies significantly across the range of experimental results.

The novel shear strength model proposed in this paper, was developed to employ a hybrid approach that integrates theoretical formulations based on the modified compression field theory (MCFT) [15] with factors derived from experimental and analytical studies to account for the influence of cross-sectional shape and fiber orientation. The MCFT serves as the foundation for numerous shear strength models for conventional concrete as well as UHPC in international design codes and specifications, including PCI Bridge Design Manual [13], AASHTO LRFD

* Corresponding author.
E-mail addresses: amjad.diab@utexas.edu (A. Diab), ferche@austin.utexas.edu (A. Ferche).

https://doi.org/10.1016/j.engstruct.2025.119654
Received 7 September 2024; Received in revised form 30 November 2024; Accepted 3 January 2025
Available online 15 January 2025
0141-0296/

Table 1
Existing shear strength models for UHPC members – the UHPC contribution.

fib Model Code (2020)	$V_{Rd,F} =$ $\left(\frac{0.18}{\gamma_c}.K.\left(100\rho_l\left(1+\frac{7.5f_{Ftuk}}{f_{ctk}}\right).f_{ck}\right)^{1/3}+0.15.\sigma_{cp}\right).b_w d$ Where: $V_{Rd,F}$ (N): Contribution of UHPC and fibers to the shear resistance in UHPC members. γ_c: Safety factor for UHPC with no fibers (recommended to be taken as 1.5). K: The size effect, taken as $1+\sqrt{200/d}$ (mm) ρ_l: longitudinal reinforcement ratio. $f_{Ftuk} = f_{R,3}/3$ (MPa), where $f_{R,3}$ is the residual flexural tensile strengths corresponding to crack mouth opening displacement of 3.5 mm. $f_{ctk} = 2.12\ln(1+0.1(f_{ck}+8))$ (MPa), where f_{ck} is the cylindrical compressive strength. σ_{cp} (MPa): Is the prestressing stress acting on the section b_w (mm): Is the minimum cross section web width d (mm): Is the effective depth of the section
AFGC (2013)	$\mathbf{V_{Rd,F} = V_{Rd,c} + V_{Rd,f}}$ $\mathbf{V_{Rd,c} = \frac{0.24}{\gamma_{cf}\gamma_E} k f_{ck}^{0.5} b_w z}$ Where: $V_{Rd,c}$ (N): Concrete contribution to the shear resistance in UHPC members. γ_{cf}: Factor for UHPC in tension and is recommended to be taken equal to 1.3. γ_E: Factor to account for uncertainty in extrapolating the model developed for UHPC and is recommended to be taken equal to 1.15. k: Is a factor to account for the prestressing effects in UHPC beams and is taken as $1+3\sigma_{cp}/f_{ck}$,for $\sigma_{cp} \geq 0$. z (mm): Effective shear depth and is taken equal to 0.9 d $\mathbf{V_{Rd,f} = \frac{A_{fv}\sigma_{Rd,f}}{\tan(\theta)}}$ Where: $V_{Rd,f}$ (N): The fiber contribution to the shear resistance in UHPC members. A_{fv} (mm^2): The effective fiber contribution area, taken equal to $b_w z$ $\sigma_{Rd,f}$ (MPa): The residual tensile strength of the fiber reinforced member. Θ (Degrees): The angle between principal compression stress and beam's horizontal axis (taken as 30^o).
PCI design guide (2021)	$\mathbf{V_{UHPC} = 1.33 \cdot f_{rr} b_v d_v \cot\theta}$ Where: f_{rr} = 5.17MPa for UHPC meeting the minimum PCI-UHPC tensile requirements. b_v (mm): Minimum web width. d_v (mm): The effective shear depth. $\theta = 29 + 3500 \bullet \varepsilon_s$, where ε_s is the net longitudinal strain at the centroid of the tension reinforcement.
AASHTO guide specifications (2024)	$\mathbf{V_{UHPC} = \gamma_u f_{t,loc} b_v d_v \cot\theta}$ Where: γ_u: Reduction factor to account for the variability in the UHPC tensile stress parameters (taken as 0.85). $f_{t,loc}$ (MPa): The localization tensile stress of the UHPC obtained from direct tension test. Θ (Degree): Is solved iteratively through the following equation for members without transverse reinforcement: $\varepsilon_{t,loc} = \frac{\varepsilon_s}{2}(1+\cot^2\theta) + \frac{2f_{t,loc}}{E_c}\cot^4\theta +$ $\frac{2\rho_{v,\alpha}f_{v,\alpha}}{E_c}\cot^2\theta(1+\cot^2\theta)\sin\alpha$ $\varepsilon_{t,loc}$: Crack localization strain of UHPC for use in design E_c (MPa): Modulus of elasticity of UHPC ρ_v: Conventional steel transverse reinforcement ratio f_s (MPa): Stress in the conventional transverse reinforcement

Bridge Design Specifications [16], Canadian Standards Association [17], and the fib Model Code [11]. In the absence of transverse reinforcement, the primary shear-resisting mechanisms in UHPC members differ from those in conventional concrete, where shear resistance largely depends on the aggregate interlock mechanism. For UHPC however, the aggregate interlock mechanism is substantially reduced due to the absence of coarse aggregates, while the presence of fiber reinforcement facilitates stress redistribution across the cracks, playing a crucial role in the shear response. The model developed in this paper incorporates these

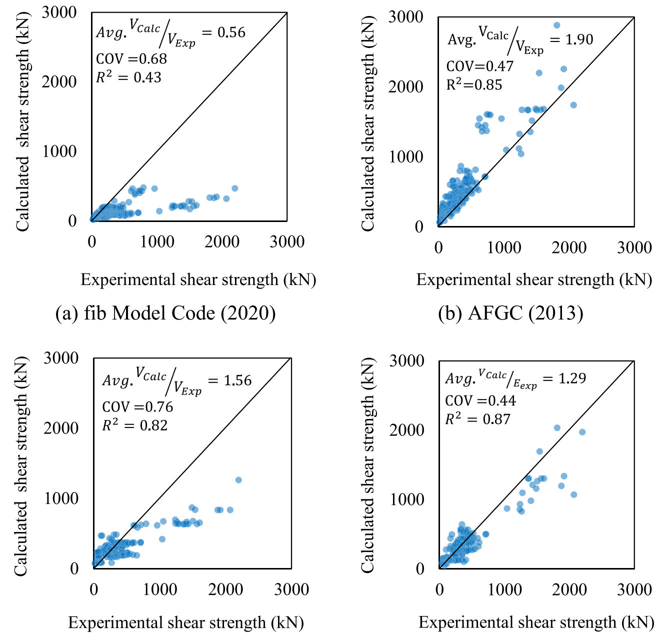

(a) fib Model Code (2020)
(b) AFGC (2013)
(c) PCI (2021)
(d) AASHTO guide specifications (2024)

Fig. 1. Performance of existing shear strength models compared to experimental data.

particularities in calculating the shear strength of UHPC members.

The accuracy of the proposed model was validated against experimental results collected from the literature. A database was assembled, containing data from 534 tests of shear-critical UHPC beams from 51 experimental studies. A significant challenge in the validation process was determining the UHPC direct tension strength, required for the shear strength model, for test programs that did not report this mechanical property. The UHPC direct tension strength was reported for only 106 out of the 534 shear tests compiled from the literature. Previous studies addressed this challenge by developing empirically-based equations to estimate the UHPC direct tension strength [18,19]. In this study, a machine learning (ML) model was employed [20], which calculates the direct tension strength of UHPC based on the mix composition. Ultimately, this study aims to advance UHPC implementation in the construction industry by offering a robust hybrid methodology, mechanics-based and data-driven, for evaluating the shear strength of UHPC members.

2. Shear-critical UHPC beams database

A comprehensive database was compiled for the validation of the proposed shear strength model, and to study key influencing factors affecting the shear strength of UHPC beams. A summary of the experimental studies included in the database and the test parameters of each study is provided in Table 2. The latest updated version of the database, including the data processing results, discussed in this section, are available online in the data repository [21]. The database contains the geometric and material properties of the specimens, in addition to key test results such as the cracking shear load (V_{cr}), experimental shear capacity (V_{exp}), and experimentally-measured inclination of the critical shear crack with respect to the longitudinal axis of the beam (θ_{exp}).

2.1. Database overview

The database includes a diverse range of cross-sectional shapes, such as I-sections, T-sections, rectangular sections, hollow-box sections, composite sections, and optimized sections. Additionally, the beams

Table 2
Database summary.

Research study	Cross section	Number of beams	Test parameters
[22]	I	7	Fiber type, fiber content, and prestressing levels
[23]	I	20	Fiber content, stirrup content
[24]	I	9	UHPC mix, fiber type, fiber content, transverse reinforcement content, long. reinforcement type, a/d ratio
[25]	I	10	a/d ratio, web opening, transverse reinforcement ratio, diagonal shear links
[26]	Rec. & I	9	long. reinforcement type, transverse reinforcement ratio
[27]	I	4	Fiber content, transverse reinforcement content
[28]	I	7	Fiber content, fiber type, a/d ratio, prestressing level
[29]	I	6	Transverse reinforcement ratio, a/d ratio
[30]	I	8	Fiber type, a/d ratio
[31]	I	12	Fiber content, a/d ratio
[32]	I	11	UHPC mix, fiber properties, curing regime, long. reinforcement type, transverse reinforcement content
[33]	I	11	Fiber content, long. reinforcement content, section shape, a/d ratio
[34]	I	4	a/d ratio
[13]	Optimized & Composite	18	Fiber type, fiber content, curing regime, prestressing level, section height, web width, transverse reinforcement ratio, a/d ratio, bursting reinforcement
[35]	I	6	UHPC mix, section height, web width, prestressing level
[36]	T	3	a/d ratio
[37]	T	7	Fiber type, fiber content, transverse reinforcement content
[38]	T	18	Cross section height, web width, a/d ratio, long. reinforcement type, long. reinforcement ratio, transverse reinforcement type, transverse reinforcement ratio
[39]	Rec.	10	fiber content, a/d ratio, long. reinforcement ratio, transverse reinforcement ratio
[40]			web width, a/d ratio, long. reinforcement type, long. reinforcement ratio, transverse reinforcement type, transverse reinforcement ratio
[39]	Rec.	10	fiber content, a/d ratio, long. reinforcement ratio, transverse reinforcement ratio
[40]	Rec.	24	Fiber type, fiber content, a/d ratio
[41]	Rec. & T-	32	Web horizontal reinforcement, transverse reinforcement ratio, fiber content, section type, transverse reinforcement angle, a/d ratio, long. reinforcement ratio
[42]	Rec.	18	Fiber content, UHPC mix, a/d ratio, long. reinforcement ratio
[43]	Rec.	12	Fiber type, fiber content, long. reinforcement ratio, transverse reinforcement ratio
[44]	Rec.	4	Transverse reinforcement ratio
[45]	Rec.	28	Section shape, long. reinforcement type, long. reinforcement ratio, a/d ratio
[46]	Rec.	16	Fiber type, fiber ratio
[47]	Rec.	10	Fiber type, fiber content, a/d ratio
[48]	Rec.	8	long. reinforcement ratio, a/d ratio
[49]	Rec.	16	Fiber content, horizontal web reinforcement ratio, long. reinforcement ratio, a/d ratio
[50]	Rec.	10	Fiber content, a/d ratio, Transverse reinforcement ratio
[51]	Rec.	5	a/d ratio, transverse reinforcement ratio
[52]	I	12	Fiber type, fiber content, a/d ratio
[53]	I	8	a/d ratio, prestressing level, transverse reinforcement ratio
[54]	Rec.	12	a/d ratio, transverse reinforcement ratio
[55]	I	8	a/d ratio, long. reinforcement ratio, transverse reinforcement ratio
[56]	T	11	Fiber type, fiber content, a/d ratio
[57]	Rec.	10	Fiber content, a/d ratio, transverse reinforcement ratio
[58]	Rec.	14	Fiber content, a/d ratio, long. & transverse reinforcement ratio, long. reinforcement type
[59]	T	13	Fiber content, a/d ratio, prestressing level, long. reinforcement ratio, transverse reinforcement ratio
[60]	Rec.	11	Fiber content, a/d ratio, long. reinforcement ratio, transverse reinforcement ratio
[61]	Hollow box	10	Fiber type, fiber content, a/d ratio, transverse reinforcement type, transverse reinforcement ratio
[62]	I	9	Fiber content, a/d ratio, section height
[63]	I	14	Fiber content, section height, prestressing level, transverse reinforcement ratio
[64]	I	2	Transverse reinforcement ratio
[65]	Rec.	8	Fiber content, a/d ratio, transverse reinforcement ratio
[66]	I	7	Prestressing levels, fiber content, fiber type
[67]	Rec.	12	Fiber content, a/d ratio, coarse aggregate effect
[68]	Rec.	6	Fiber content, a/d ratio
[69]	Rec.	6	Fiber content, size effect
[70]	Composite		2 a/d ratio
Total number of beams		**538**	

included in the database had various fiber reinforcement properties, prestressing levels, reinforcement ratios (longitudinal and transverse), shear-span-to-depth (a/d) ratios, web openings, curing regimes, and cross-sectional variations. An overview of the characteristics of the database is shown in Fig. 2. It can be seen that 68 % of the beams in the database do not have conventional transverse steel reinforcement, and 26 % are prestressed. Regarding the cross-sectional characteristics, 53 % have rectangular cross sections, 35 % have I-sections, 6 % are T-section beams, and 6 % include other types such as box-girders, composite sections, and optimized I-sections. Among all beams, 81 % had straight fiber reinforcement, 9 % had a combination of straight and hooked fiber reinforcement, 3 % used only hooked fibers, and 7 % incorporated other types, such as organic, polyethylene, and basalt fibers.

The main failure modes observed experimentally in UHPC beams are diagonal tension failure, shear compression failure, and diagonal compression failure, as defined by Zhang et al. (2024) [69]. Diagonal tension failure (DTF) occurs when the tensile stresses along a diagonal crack exceed the UHPC tensile strength, leading to the formation and propagation of diagonal cracks, as shown in Fig. 3(a) [69]. Shear compression failure (SCF) results from a combination of high shear and compression stresses, resulting in crushing of the UHPC in the web region, accompanied by opening of diagonal cracks, as shown in Fig. 3(b) [69]. Diagonal compression failure (DCF) develops when the compressive stresses along a diagonal crack path exceed the concrete's compressive strength, leading to steep diagonal cracks accompanied by crushing along the beam's compression strut as shown in Fig. 3(c) [69]. The primary differences lie in the governing failure mechanisms: diagonal tension failure is governed by the tensile stresses, shear

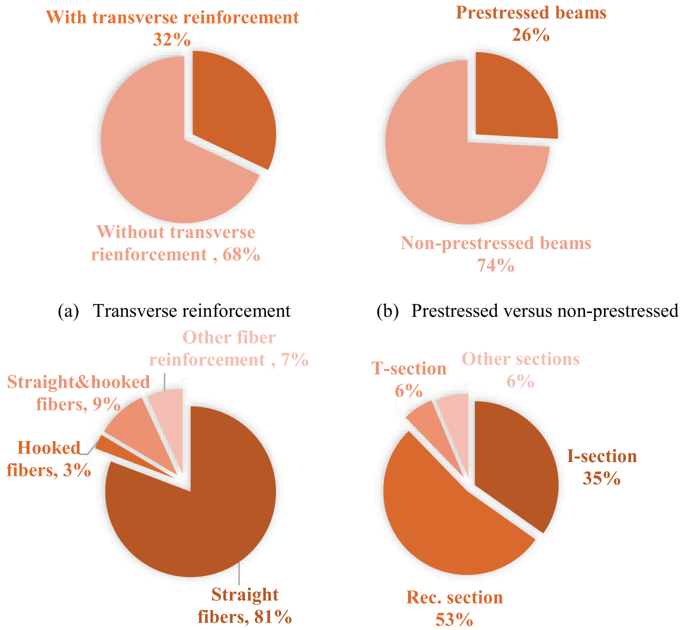

(a) Transverse reinforcement (b) Prestressed versus non-prestressed

(c) Fiber reinforcement type (d) Section type

Fig. 2. Database characteristics overview.

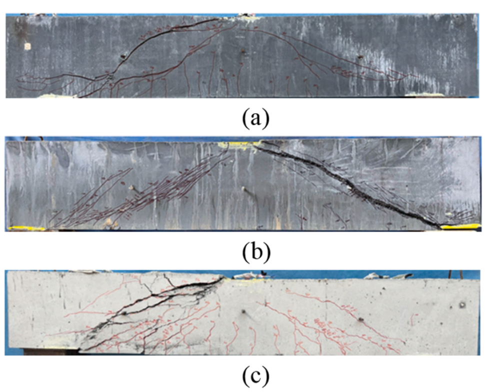

(a)

(b)

(c)

Fig. 3. Illustration of typical crack patterns for various shear failure modes (a) Diagonal tension failure (b) Shear compression failure (c) Diagonal compression failure [69].

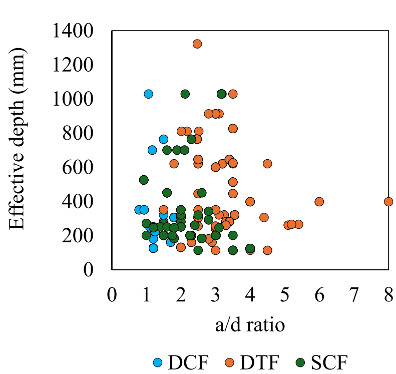

Fig. 4. Shear failure mechanisms across different shear-span-to-depth (a/d) ratios and effective depths (d).

compression failure by combined shear and compressive stresses, and diagonal compression failure by high diagonal compressive stresses [71, 72].

Fig. 4 summarizes the different types of shear failure modes for the beams in the database, across different shear-span-to-depth (a/d) ratios and effective beam depths (d). It can be observed that DCF is generally prevalent in shear-critical beams with a/d ratios lower than 2.0, while DTF mainly occurs in shear-critical beams with a/d ratios greater than 2.0. Lastly, SCF occurs in beams with a/d values ranging from 1.0 to 4.0.

A frequency distribution analysis of the database is presented in Fig. 5. The analysis indicates that most of the shear-critical UHPC beams have an a/d ratio less than 4.0. Additionally, the majority of the beams have a height of less than 500 mm and web widths less than 175 mm, with a large number of beams having web widths as thin as 50 mm. The majority of the beams had web heights less than 400 mm. The UHPC compressive strength (f'_c) ranged between 100 and 225 MPa and the UHPC direct tension strength (f'_t) followed a similar distribution to the compressive strength with values ranging between 5 and 16 MPa. The cracking shear load (V_{cr}) ranged from 50 and 400 kN, while the ultimate shear resistance (V_u) had values between from 100 and 4000 kN. Lastly, the experimental value of the inclination of the critical shear crack with respect to the longitudinal axis of the beam (θ_{exp}) values ranged between 20°and50°.

2.2. Geometric properties

The database includes a wide range of cross-sectional geometries. To ensure consistency across different experimental programs, the terminology defined in Fig. 6 was used to describe the cross-sectional properties of the specimens. Therefore, b_{tf} represents the top flange width, h_{tf} is the top flange height, h_{tt} is the top transition height, b_{tt} is the top transition width, h_w is the height of the web, b_w is the minimum web width, h_{bt} is the bottom transition height, b_{bt} is the bottom transition width, b_{bf} is the bottom flange width, h_{bf} is the bottom flange height, and H is the height of the cross section.

2.3. Compressive strength

The database includes the UHPC compressive strength (f'_c) of the beam specimens, as measured from tests on cubes and cylinders of varying sizes. To standardize these values across the dataset, conversion factors developed in previous studies were applied [73,74]. This approach enabled the conversion of all compressive strength measurements to equivalent standard compressive strength values as measured on 100×200 mm cylinders, ensuring uniformity across the dataset. Table 3 provides the conversion factors used for the specimens based on their shape and geometry.

2.4. Tensile strength

Previous research has shown a significant correlation between the shear behavior of UHPC beams and the uniaxial tension behavior of the UHPC material, characterized through direct tension tests [66,75]. This is due to the direct tension test's accurate representation of the tensile stress state in the critical shear region in UHPC members, unlike other tests such as the flexural tension test results. However, a major challenge in further evaluating this relationship has been the limited availability of experimental programs conducting direct tension tests to characterize the uniaxial tension response of UHPC [18]. To overcome this limitation, the authors have previously developed a machine learning (ML) model that calculates the direct tension characteristics of UHPC mixes based on their specific mix design [20], including the tensile cracking stress (f_{cr}), peak direct tension strength (f'_t), and strain at peak direct tension strength (ε'_t). The ML-predicted direct tension strength values are included in the database for the tests that did not report this property, which was instrumental in the validation of the shear strength model. Data for each test is explicitly annotated indicating whether the direct tension test results were obtained from actual experimental

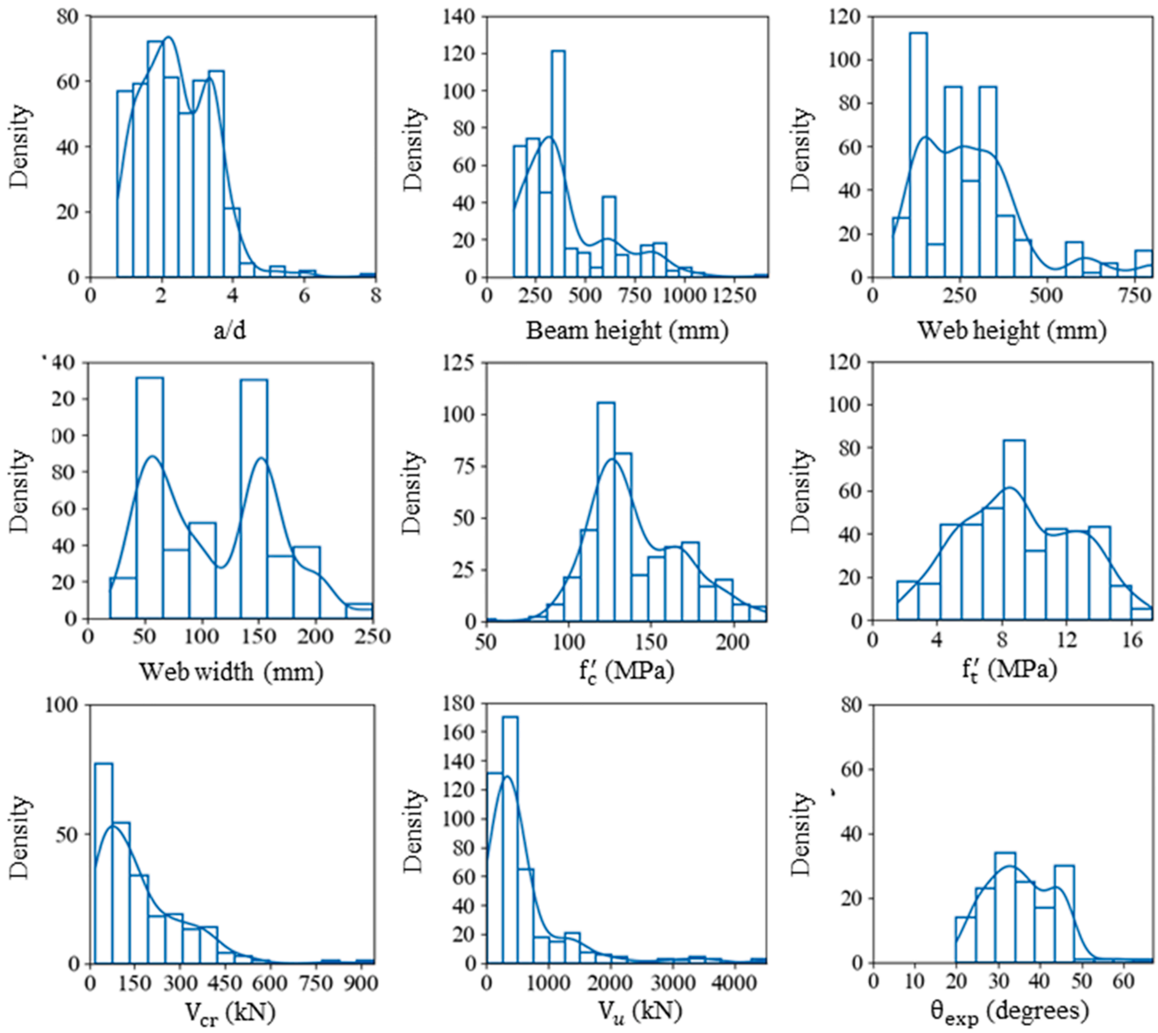

Fig. 5. Frequency analysis of the UHPC beams in the database.

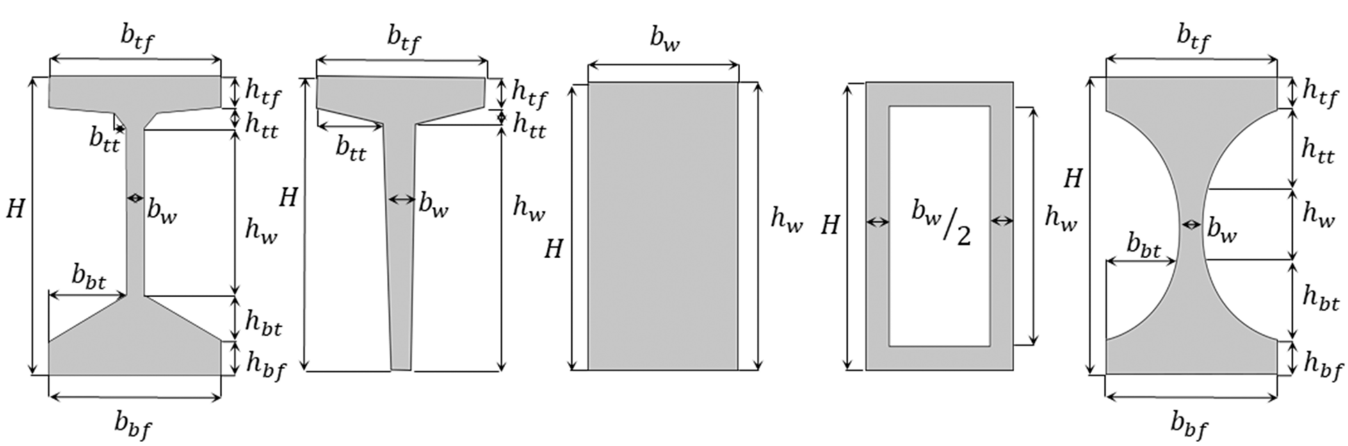

Fig. 6. Geometric properties of UHPC beams in the database.

measurements or estimated using the ML algorithm [20].

2.5. Longitudinal reinforcement

The database also includes comprehensive details on the longitudinal and transverse reinforcement for each beam, including the reinforcement area and yield strength for both mild reinforcing steel and the prestressed reinforcement. Currently, it contains only prestressed UHPC members and does not contain any post-tensioned members.

For experimental programs that reported prestressing forces and losses, these values were directly extracted. In cases where such values were not reported, the prestressing forces were estimated based on a prestressing stress of 75 % of the specified tensile strength of prestressing steel (f_{pu}) which conforms with AAHSTO specifications [16]. In

Table 3
Conversion factors for $f_c^{'}$ to standard 100 × 200 mm cylindrical specimen [73,74].

Specimen type	Cube	Cube	Cube	Cube	Cube	Cylinder	Cylinder	Cylinder	Cylinder
Dimensions (mm)	150	100	70	50	40	50 × 100	75 × 150	100 × 200	150 × 300
Conversion factor	1.10	0.98	0.92	0.94	1.10	1	1	1	1.04

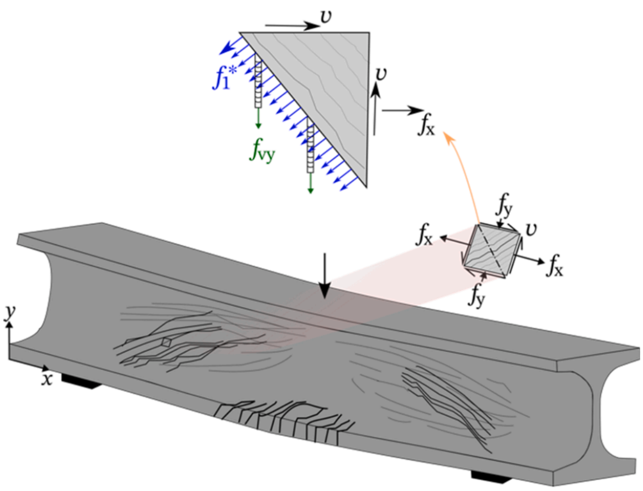

Fig. 7. Stresses in a shear-critical beam.

addition, prestressing loss was estimated following an approach that accounted for immediate and time-dependent losses such as elastic shortening (ε_{es}), UHPC shrinkage strain (ε_{sh}), and relaxation of prestressing steel (Δ_{fp}). The net longitudinal tensile strain in the section at the centroid of the tension reinforcement (ε_s) was calculated as:

$$\varepsilon_s = \frac{P^*_{p_{bot}}}{A_{p_{bot}}E_{p_{bot}}} + \frac{P^*_{p_{top}}}{A_{p_{top}}E_{p_{top}}} - \varepsilon_{es} - \quad \varepsilon_{sh} \tag{1}$$

$$\varepsilon_{es} = \frac{P_{p_{bot}} + P_{p_{top}}}{A_c E_c} \tag{2}$$

where $P^*_{p_{bot}}$ and $P^*_{p_{top}}$ are the bottom and top effective prestressing forces after relaxation, $A_{p_{bot}}$ and $A_{p_{top}}$ are the bottom and top cross-sectional areas of the prestressed reinforcement, and $E_{p_{bot}}$and $E_{p_{top}}$are the Youg's modulus of elasticity for the bottom and top prestressed reinforcement, respectively. The effective prestressing forces, $P^*_{p_{bot}}$ and $P^*_{p_{top}}$, are assumed equal to 0.95 of the initial prestressing force, This value was based on the relaxation from prestressing the strands at 75 % of f_{pu} and testing conducted 28 days after beam preparation [76]. A_c is the gross corss-sectional area, and E_c is the modulus of elasticity of concrete.

Based findings from literature, an average 28-day value of 0.5×10^{-3} was used for the shrinkage strain, ε_{sh}, common for UHPC mixes because of low water-to-cement (w/c) ratios and lack of coarse aggregate [77, 78]. This value was applied for all specimens, except for the beams that were reported to have had post-curing thermal treatment.

3. Shear strength model for UHPC members

The proposed approach bears similarity with the simplified modified compression field theory [79], and El-Helou & Graybeal model for shear-critical UHPC members [80]. It introduces new parameters to explicitly account for the cross-sectional shape effect and fiber orientation. In addition, the model proposes a simplified approach for calculating the inclination of compressive stresses. These enhancements improve the accuracy and applicability of the model for predicting the behavior of shear-critical UHPC members.

The recent industry trends of using UHPC beams with cross sections of varying widths across the height, as shown in Fig. 6, motivated this study to investigate the effect of cross-sectional shape on the behavior of shear-critical UHPC beams. The MCFT, originally formulated for membrane elements with uniform thickness, was adapted here through an analytical study utilizing nonlinear finite element analysis (NLFEA) formulation to examine the effects of varying cross-sectional widths along the height and to evaluate the shape effect on the behavior of shear-critical UHPC beam [81].

Previous experimental programs have also demonstrated that various factors – such as casting methods, beam dimensions, and the rheology of the UHPC mix – can induce significant fiber orientation effects in UHPC beams [82]. These factors collectively influence the alignment of fibers, which in turn affects the isotropy of the UHPC material [83–85]. Despite this evidence, existing models typically address fiber orientation by simplifying the issue, often incorporating only a fraction of the direct tension strength of UHPC to account for these effects. In contrast, the proposed model offers a more comprehensive approach by integrating key parameters that significantly impact fiber orientation. Specifically, the shear strength model presented in this study introduces a detailed fiber orientation component. This component accounts for both the height of the UHPC beam (H), and the ratio of web width (b_w) to the maximum fiber length (l_f).

3.1. *The cross-sectional shape effect on the shear strength of UHPC members*

The model specifically addresses the behavior of an element located in a region of a shear-critical UHPC beam shown in Fig. 7. With the fundamental assumption that the shear stresses are constant over the effective depth, this element can be facilitated to calculate the shear strength employing equilibrium equations, compatibility conditions, and constitutive relationships. The constitutive models employed were previously developed by the authors to reflect the behavior of the UHPC material [81].

The shear strength model proposed in this paper is based on strain compatibility and equilibrium conditions expressed for a rectangular membrane element with uniform thickness, as shown in Fig. 7. A basic assumption of this model, which conforms with the simplified MCFT, [79] is that the clamping stresses (f_y) in the beam's critical shear region are negligible, as shown in Fig. 7. The model also assumes that the conventional transverse reinforcement reaches yield state (f_{vy}) at ultimate shear strength, in UHPC beams that are not governed by concrete crushing; the validity of this assumption is further discussed in the subsequent sections. Based on these assumptions, the shear stresses (v) acting on the element shown in Fig. 7 at ultimate strength can be expressed as:

$$v = f_1^* \cot\theta + \rho_v f_{v_y} \cot\theta \tag{3}$$

Where f_1^* is the effective principal tensile strength, which is a function of the direct tension strength and the fiber orientation, ρ_v is the conventional steel reinforcement ratio in the y-direction, and f_{v_y} is the yield strength of the conventional steel reinforcement in the y-direction.

A previously developed NLFEA approach which is based on the MCFT formulations was utilized to analyze the shape effect in shear-critical UHPC beams [81]. Fig. 8 summarizes the model's formulation and its validation procedure using UHPC panels and shear-critical beams reported in the literature. A more comprehensive information on the

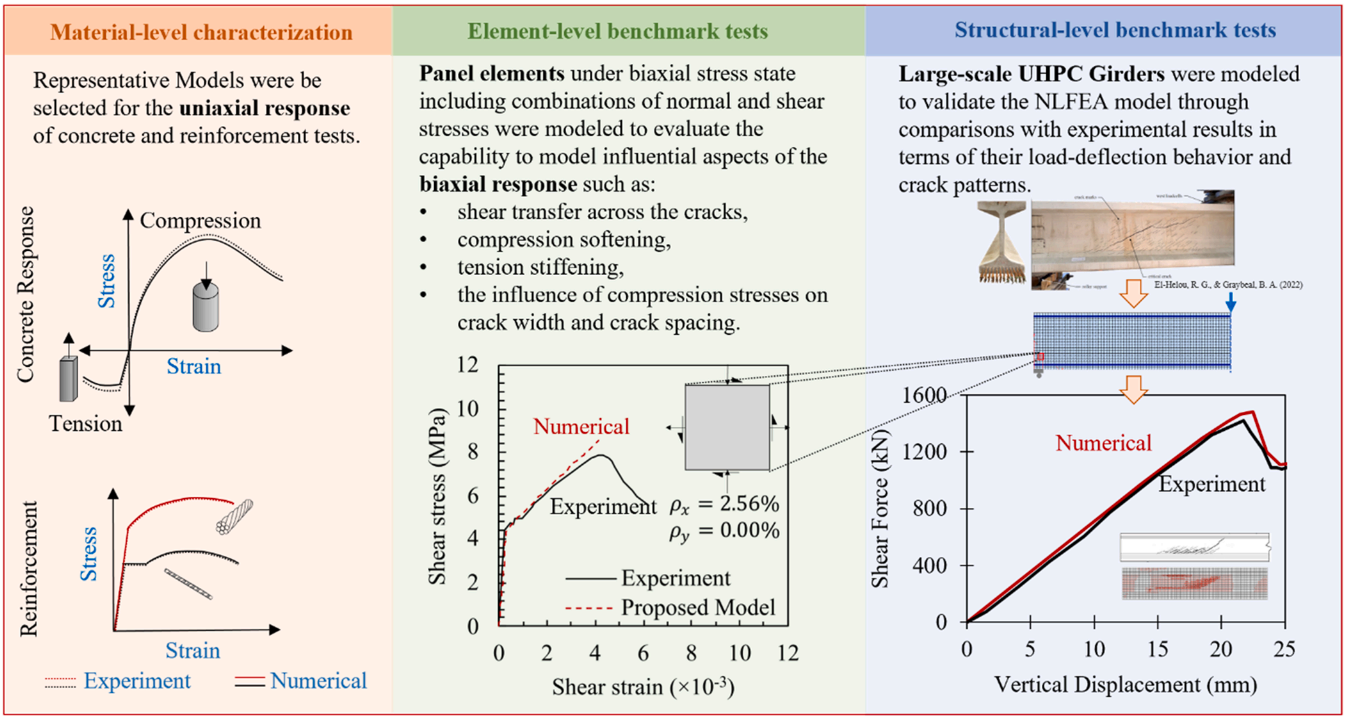

Fig. 8. NLFEA validation process using UHPC panels and shear-critical beams reported in the literature [81,86,87].

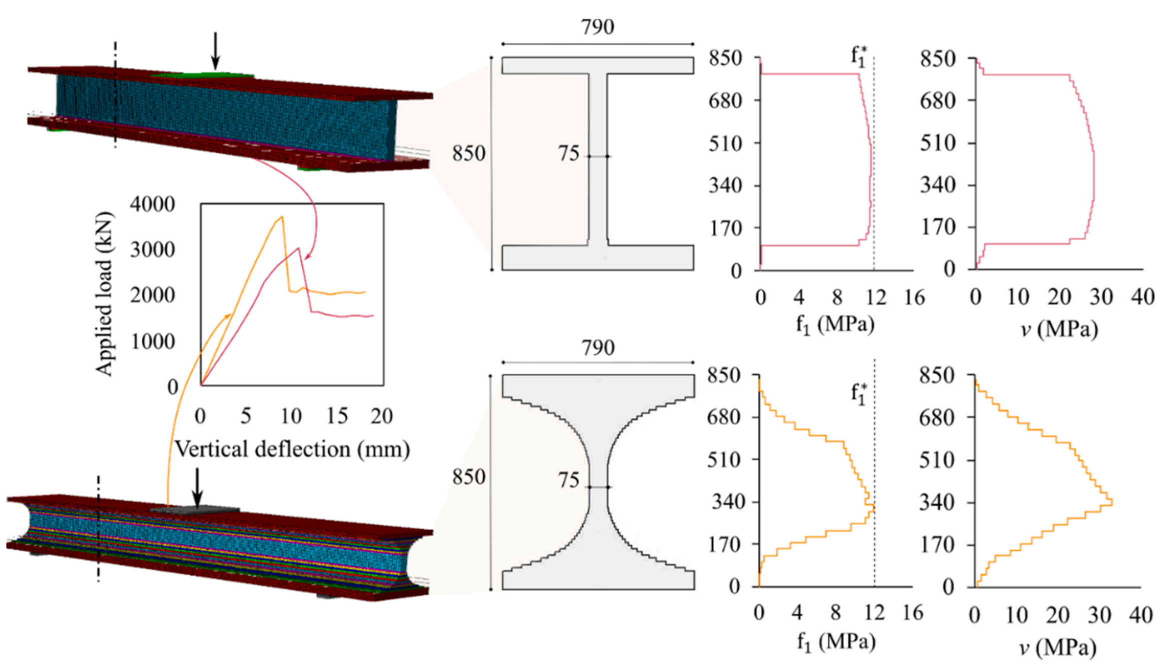

Fig. 9. Shear stresses and principal tensile stresses profiles at peak load (dimensions shown in mm).

formulation and validation of the NLFEA approach is provided in a separate publication by the authors [81].

NLFEA was utilized to analyze the distribution of shear and principal tensile stresses in the critical shear section, at a distance (d_v) away from the support in a conventional I-section and optimized sections with varying thicknesses, as shown in Fig. 9. The analysis results show that for sections with varying thicknesses, the assumption originally adopted by the MCFT provisions of having an approximately constant shear and tensile stresses along d_v is not valid. As a result, the terms v and f_1^* in Eq. 3 vary along the depth of the shear-critical UHPC section to become

$$v(y) = f_1(y)\cot\theta + \rho_v f_{v_y}\cot\theta \quad (4)$$

where $v(y)$ and $f_1(y)$ are the shear stresses and effective principal tensile stresses measured at a depth (y) from the bottom of the beam.

For the case of conventional UHPC sections, V_{UHPC} is calculated by multiplying the term $f_1^*\cot\theta$ by the cross-sectional area contributing to the shear resistance, $b_v d_v$, V_{UHPC} becomes

$$V_{UHPC} = f_1^* b_v d_v \cot\theta \quad (5)$$

However, for optimized sections, since f_1 is not constant across d_v,

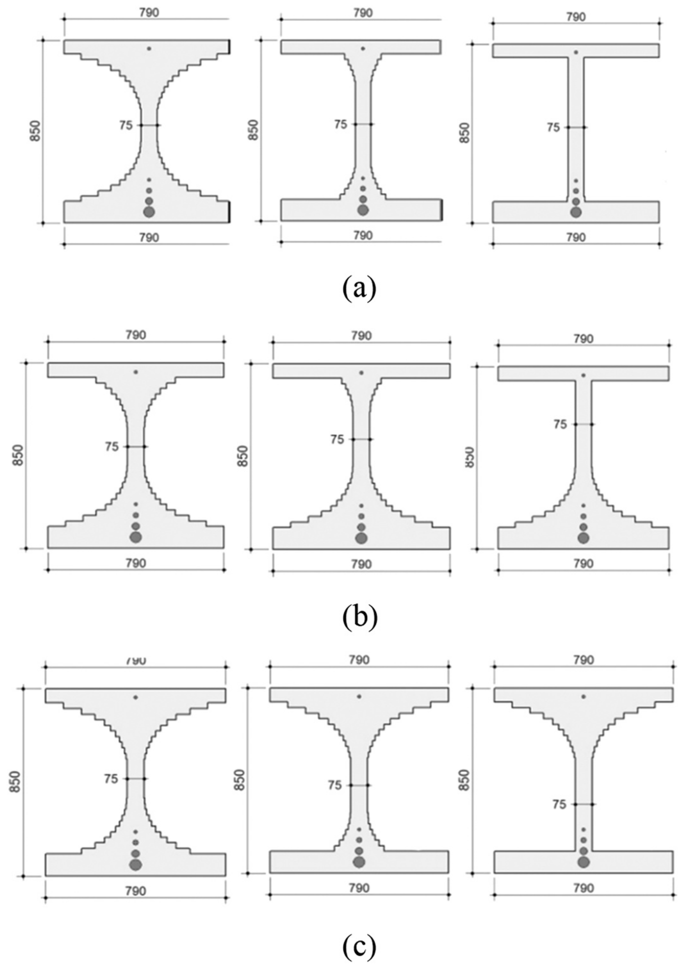

Fig. 10. Cross-sectional variation considered for the analysis of shape effect: (a) Transition from both the top and bottom (b) Transition from the top (c) Transition from the bottom (dimensions in mm).

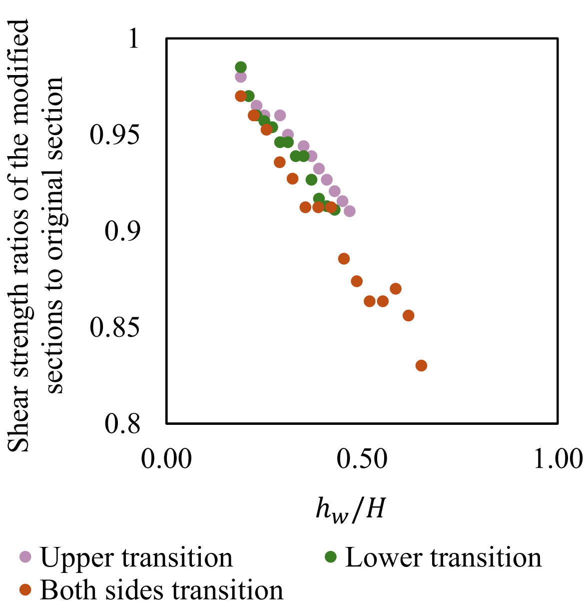

Fig. 11. Analytical shear strength ratios of the specimens with cross-sectional transition to the control specimen.

determining V_{UHPC} requires the calculation of the area extending throughout d_v between the centroids of the resultant internal tension force (y_t) and compression force (y_c), leading to the following expression:

$$V_{UHPC} = d_v \cot\theta \int_{y_t}^{y_c} f_1(y) b_w(y) dy \tag{6}$$

Where $f_1(y)$ is the principal tensile stress at depth y in the beam and $b_w(y)$ is the web width at depth y in the beam.

An analytical study was conducted based on shear-critical tests reported in the literature, with details on the physical and mechanical properties of the specimens provided in the shear-critical beams database [13,21]. This study aimed to evaluate the shape effect on the behavior of beams using the NLFEA approach previously developed [81]. The study was conducted by gradually reducing the transition between the web and the flange regions and comparing the results with the control specimen with no change in the transition region, as shown in Fig. 10. The analytical study was structured into three distinct phases:

(a) Simultaneous Transition Alteration: In this initial phase, modifications were made to both the bottom and top transitions concurrently.
(b) Top Transition Alteration: The second phase of analysis focused solely on adjusting the top transition.
(c) Bottom Transition Alteration: The final phase focused on modifying only the bottom transition.

Shown in Fig A.1 in the appendix are the results presented in terms of the shear strength ratios of the modified to the original section and the web width to full height ratios. The results show a general trend of shear capacity decrease for all transition cases, indicating that the bottom transition has a more significant influence. The plots also show that the shear capacity stabilizes beyond a certain h_w/H, as the transition falls outside the effective shear depth and thus exerts minimal influence on shear capacity. The average results compared to the control models are shown in Fig. 11 for the analyzed shear-critical beams.

Based on the results shown, the average results compared to the specimen with no transitions between the web and the flange are shown in Fig. 12. Based on these results, a simplified parameter was introduced in this study to characterize the shape effect on the behavior of shear-critical UHPC beams based on the trend line for the average results. This parameter, is denoted as "ζ," and is expressed as:

$$\zeta = 1.27 - \frac{1}{3} h_w \Big/ H \leq 1.2 \tag{7}$$

The shape effect factor was set to be less than 1 when h_w/H for beams with rectangular cross sections. This adjustment increases the model's conservatism, aligning with findings from previous studies. These studies highlighted that flanges in certain sections provide confinement in shear-critical UHPC beams, optimizing the strain at peak tensile strength—a benefit absent in hollow box and purely rectangular sections [66,87]—a benefit which is not present in hollow box and rectangular sections.

3.2. The fiber orientation effect on the shear strength of UHPC members

The efficacy of fiber reinforcement in UHPC is influenced not only by the fibers' physical properties but also by their orientation. The orientation of the fibers significantly influences the isotropy of the UHPC members [88], potentially causing variations in the mechanical properties. One of the main factors affecting the orientation of fibers in UHPC members is known as the wall effect. This effect stems from a geometric constraint where fibers are restricted from free rotation at distances less than half of the fiber's length away from the formwork [82]. This results in a parallel fiber orientation near any solid boundary within the

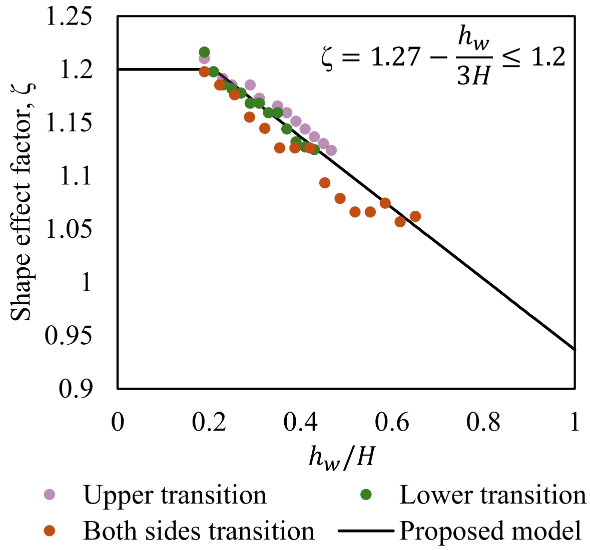

Fig. 12. Comparison between the trend line of the analytical shear strength ratios of the specimens with cross-sectional transition to the control specimen and the proposed model.

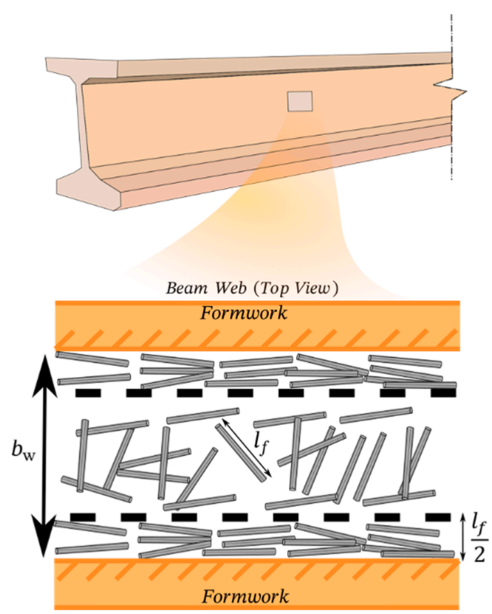

Fig. 13. Wall effect on the orientation of fiber reinforcement in UHPC beams webs.

material flow. Fig. 13 provides a visual depiction of how the wall effect influences fiber orientation in the web regions of UHPC beams. This effect increases as the beam web thickness decreases.

Previous experimental programs also illustrated that the fibers are mainly oriented in the horizontal plane rather than the transverse direction. Nevertheless, fibers tend to orientate towards the transverse direction as the depth of the beam increases [82,88]. Following these observations, a comprehensive analysis of the fiber orientation effect was conducted based on the web width, average fiber length, and the overall member height, summarized in the following sub-section and resulting in the implementation of a fiber orientation parameter to the shear strength model proposed in this paper.

3.3. Proposed shear strength model

The nominal shear resistance (V_n) of UHPC beams is calculated as:

$$V_n = V_{UHPC} + V_s + V_p \leq V_{n_{max}} + V_p \tag{8}$$

$$V_{UHPC} = \zeta\varphi\psi f'_t b_w d_v \cot\theta \tag{9}$$

$$V_S = \frac{A_v f_{vy}}{s} d_v \cot\theta \tag{10}$$

$$V_{n_{max}} = 0.25 f'_c b_w d_v \tag{11}$$

Where: V_{UHPC} is the nominal shear contribution of UHPC, V_s is the shear resistance provided by the transverse reinforcement, V_p is the component of prestressing force in the direction of the shear force, $V_{n_{max}}$ is the maximum nominal shear resistance governed by UHPC crushing, d_v is the effective shear depth taken as the distance between the resultants of the tension and compression forces due to flexure, this value is taken as the maximum between 0.9d and 0.72H, where d is the effective depth from extreme compression fiber to the centroid of the tension force in the tension reinforcement, b_v is the effective web width taken as the minimum web width within d_v, θ is the angle of inclination of diagonal compressive stresses, f_{vy} is the yield strength of the conventional transverse reinforcement, A_v is the area of transverse reinforcement, and f'_c is the compressive strength of the UHPC strength incorporated in the shear-critical member.

The maximum nominal shear resistance, $V_{n_{max}}$, is an upper limit on the strength, originally proposed in the simplified MCFT for conventional concrete members and adopted for shear-critical UHPC members governed by web crushing in the FHWA AASHTO guide specifications [79]. This specification is based on a conservative compression softening assumption of 0.5 f'_c under biaxial tension-compression stresses, this value is similar to the value proposed by the authors in a previous study [81], assuming a strain at peak compressive strength value (ε'_c) of −0.0035 for UHPC mixes [80].

The fiber orientation factor, φ, was developed through regression analysis. This analysis, summarized in Fig. 14, considered the relationship between the ratio between the experimental shear strengths and the nominal ones determined analytically with the proposed model (without φ) across various (b_w/l_f) and (H) values. The coefficients were determined by optimizing the fit between the calculated and experimental data. Based on this analysis, the proposed expression for φ is given by:

$$\varphi = \left(1 - 0.2\frac{H}{1000}\right)\left(1 - 2\frac{b_v/l_f}{1000}\right) \tag{12}$$

In a similar manner, a size effect factor (ψ) was adopted for UHPC members with no fiber reinforcement, similar to the model proposed in a previous study by other researchers [89]. This factor addresses the relationship between the calculated shear strength (without considering size effects) and experimental results, as depicted in Fig. 15. The analysis demonstrates that ψ effectively adjusts the predicted shear strength to account for variations in d_v. Based on the analysis results, the size effect factor is expressed as:

$$\psi = \frac{1300}{1300 + d_v} \tag{13}$$

3.4. Determination of the diagonal compressive stresses inclination angle

The next step in the design process is to determine θ as a function of the axial strain at the mid web region in the critical shear section, ε_x. A compatibility-based expression was derived in a previous study by others, combining the compatibility relationships to determine ε_x based on multiple input parameters including ε'_t, f'_t, E_c, and the stress in the transverse reinforcement in the y-direction (f_{sy}) [80]. By assuming that

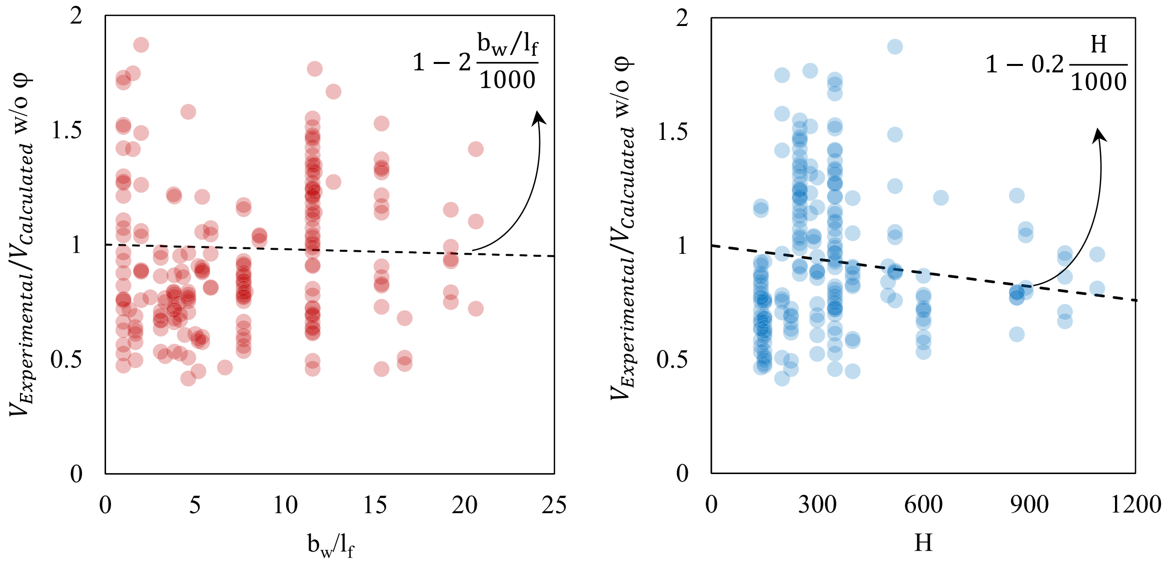

Fig. 14. Empirical derivation of the fiber orientation coefficient, φ, in terms of the beam dimensions and fiber reinforcement length.

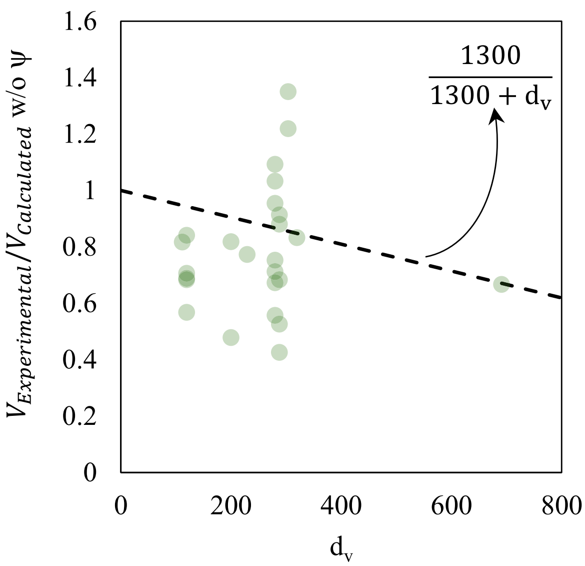

Fig. 15. Empirical derivation of the size effect factor, ψ, in terms of the beam effective shear depth.

Table 4
Properties of the UHPC specimens (El-Helou & Graybeal 2022).

ID	f'_c MPa	f'_t MPa	f_{cr} MPa	ε'_t $\times 10^{-3}$	b_w mm	H mm	$A_{P_{bot}}$ mm^2	a/d -
H-P1	137.0	11.3	10.5	3.7	76	889	4552.8	3.5
J-P1	158.0	8.6	7.9	5.2	76	889	4552.8	3.5
J-P1S	152.0	9.3	8.9	4.4	102	889	3414.6	3.5
H-P2	140.0	10.7	10.8	3.2	76	889	4552.8	3.5
H-P3	158.0	10.9	10.6	2.8	76	1092	4552.8	3.5

Notes: f'_c: UHPC compressive strength; f'_t: UHPC tensile strength; f_{cr}: UHPC cracking stress; ε'^{a}_t: UHPC strain at peak tensile; b_w: Web width; **H**: Height; $A_{P_{bot}}$: Prestressed steel reinforcement area; a/d: Shear-span to depth ratio.

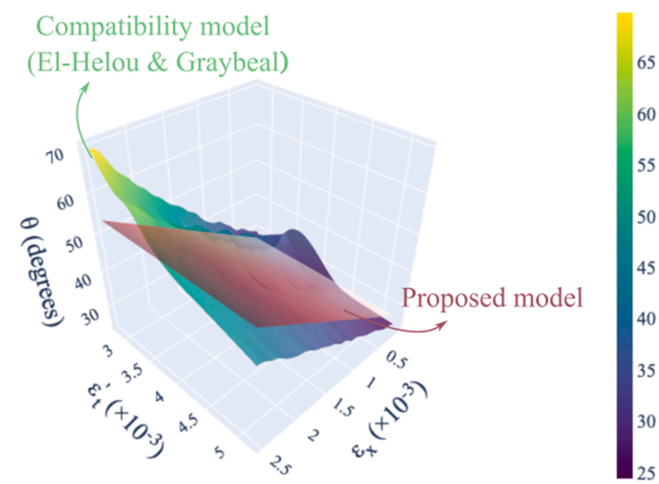

Fig. 16. Comparison between the compatibility model results for calculating θ and the proposed simplified model results.

the compressive stresses remain at the elastic stage at shear failure, the following relation relates the cracking angle with ε_x

$$\varepsilon'_t = \varepsilon_x(1 + \cot^2\theta) + \frac{f'_t}{\alpha E_c}\cot^4\theta + \frac{\rho_y f_{s_y}}{\alpha E_c}\cot^2\theta(1 + \cot^2\theta) \tag{14}$$

where f_{s_y} is assumed equal to f_{y_y} in this study, and α is a factor to account for the compression softening effect on the compressive strain in UHPC composites. Previous studies showed that compression softening has minimal effect on the compressive strain, as such, in this study, α was set equal to 1 [81,90].

Eq. 15 was used to estimate θ for the beams tested by El-Helou & Graybeal (2022) [87], a total of six shear-critical bulb-tee pretensioned bridge girder specimens were loaded until failure. These girders were constructed using two different UHPC mixes from separate concrete plants. The mixes were labeled as mix "H" and mix "J," both containing 2 % steel fibers by volume. Four of the girders were 9.75 m long and 0.90 m high, while the other two measured 11.60 m in length and

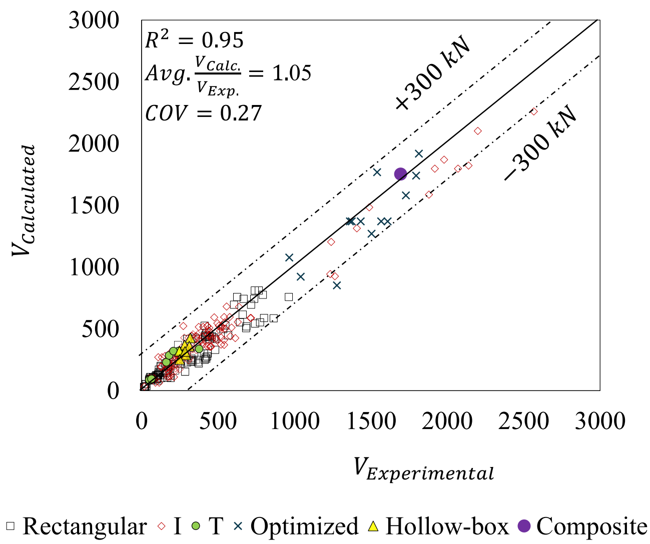

Fig. 17. Comparison between calculated and experimental shear strengths for various cross sections.

1.10 m in height. The study explored various factors crucial to the shear design of UHPC bridge girders, such as the mechanical properties of different UHPC mixes, girder height (ranging from 0.90 to 1.10 m), web width (0.08–0.1 m), bottom prestressing area ($A_{p_{bot}}$) (0–4522 mm^2), and the addition of vertical steel reinforcement in the web (0.00–1.29 %). The research aimed to evaluate how these variables affected the shear performance of UHPC girders. Table 4 provides a summary of the specimens included in this validation study.

Fig. 16 presents a 3D contour plot illustrating the relationship between the beams' mechanical properties and θ to different values of ε_x and ε_t'. The first part of the plot was generated using interpolated surface data obtained from the calculated results from Eq. 15 for the beams in Table 4. The second part of the plot, represented by a plane surface, corresponds to the simplified model developed by the authors. This model, formulated through regression analysis based on the outputs of Eq. 15, provides an accessible and practical means to estimate θ while maintaining reasonable accuracy. This regression-based approach balances computational efficiency with usability, making it particularly beneficial for engineering applications where simplified calculations are preferred. Therefore, the inclination of the diagonal compressive stresses, θ, is calculated as:

$$\theta = 26 + 11000\varepsilon_x \tag{15}$$

The shear stresses are assumed to be uniform over the effective shear depth in this model. The highest longitudinal strain ε_x can be approximated as the strain in the flexural tension reinforcement [91]. The determination of ε_x is calculated as

$$\varepsilon_s = \frac{\left(\frac{|M_u|}{d_v} + 0.5N_u + |V_u - V_p| - A_{ps}f_{po} - \gamma_u f_{t,cr} A_{ct}\right)}{E_s A_s + E_p A_{ps}} \tag{16}$$

In the case where the ε_s is negative or is less than the cracking tensile strain ($\varepsilon_{t,cr}$), the value of ε_s is recalculated as:

$$\varepsilon_s = \frac{\left(\frac{|M_u|}{d_v} + 0.5N_u + |V_u - V_p| - A_{ps}f_{po}\right)}{E_s A_s + E_p A_{ps} + E_c A_{ct}} \tag{17}$$

Table 5
Performance indicators of the proposed model for the different section types.

Section	Avg. $\frac{V_{Calculated}}{V_{Experimental}}$	COV	R^2
Rectangular	1.04	0.29	0.87
I	1.09	0.28	0.96
T	1.40	0.16	0.83
Optimized	0.99	0.12	0.71
Hollow box	1.22	0.12	0.54

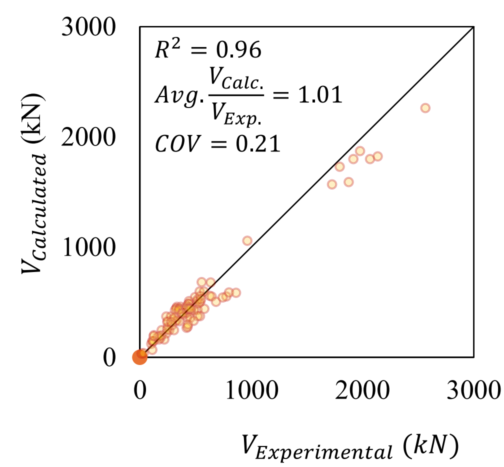

Fig. 19. Comparison between shear design model calculation results and experimental data results for transversely reinforced shear-critical UHPC beams.

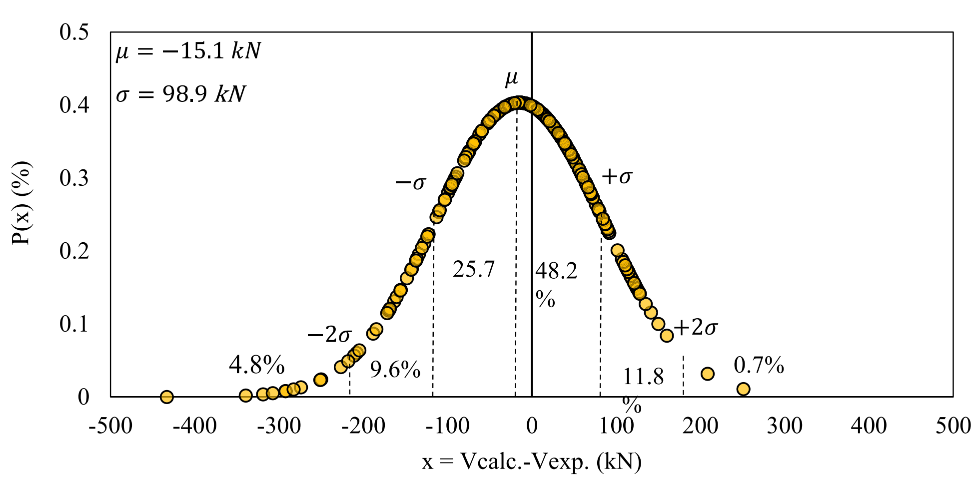

Fig. 18. Comparison between $V_{calc.}$ and $V_{exp.}$ with normal distribution of errors.

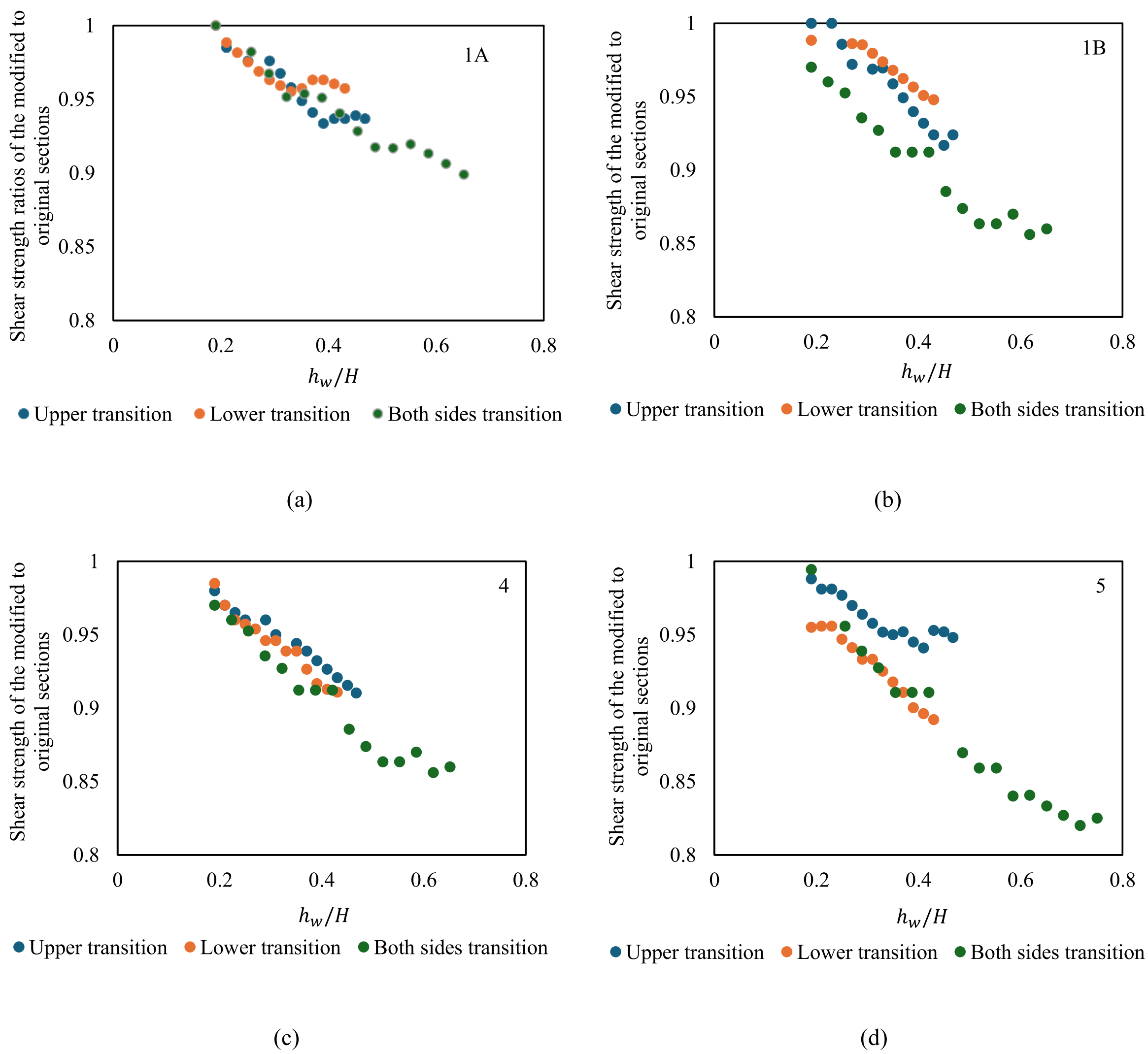

Fig. A.1. Parametric analysis results for the shape effects for beams tested by Tadros et al. [13].

where: $|M_u|$ is the absolute value of the moment at the section, not taken less than $|V_u - V_p|d_v$, N_u is the factored axial force, V_u is the factored shear force acting of the section, V_p is the prestressing force component parallel to the shear loading direction taken positive if resisting the applied shear load, A_{ps} area of prestressing steel on the flexural tension side of the member, and f_{po} is a parameter taken as the modulus of elasticity of prestressing steel multiplied by the locked-in difference in strain between the prestressing steel and the surrounding UHPC. E_s is the modulus of elasticity of the nonprestressed steel reinforcement, A_s and A_{ct} are the areas area of non-prestressed steel on the flexural tension side of the member at the section, and the area of UHPC on the flexural tension side of the member, respectively. The value of ε_x is taken equal to $0.5\times\varepsilon_s$ for simplification purposes.

4. Model validation

The accuracy of the model was evaluated by comparing the nominal shear strength values of members in the database with the analytical results calculated using the novel model developed. UHPC members with a/d ratios less than 2.0 were excluded, as their behavior aligns with deep beam action, making sectional analysis methods unsuitable for accurately predicting their shear strength.

In the process of calculating θ for the members in the database, M_u was calculated at the critical shear crack location assumed to be at a distance equal to d_v away from the applied point load. As shown in Fig. 17, the proposed model had reasonable accuracy in predicting the shear strength for the shear-critical UHPC members in the database, including members with different cross sections, reinforcement types, and fiber reinforcement types with an R^2 equal to 0.95, an average calculated-to-experimental results ratio (Avg. $V_{calc.}/V_{exp.}$) of 1.05, and a coefficient of variation (COV) equal to 0.27. The results show that the proposed model predicted results are within a ±300 kN interval within the experimental capacity.

Fig. 18 presents a detailed analysis of the error distribution of the difference between V_{calc} and V_{exp} which is denoted as (x) in the figure, the results showed that the mean x value (μ) is equal to −15.1 kN and the standard deviation (σ) is equal to 98.9 kN, the results indicates that 73.9 % of the errors fall within one standard deviation of the mean, 21.4 % lie between one and two standard deviations away from the mean, and only 5.5 % exceed two standard deviations. This distribution suggests a strong concentration of data around the mean, with minimal outliers, reinforcing the reliability of the predictive model. The corresponding probability density function (P(x)) for each point is calculated as:

$$P(x) = \frac{1}{\sigma\sqrt{2\pi}}\exp\left(-\frac{(x-\mu)^2}{2\sigma^2}\right) \tag{18}$$

Table A.2
UHPC shear-critical beams database Key parameters characteristics.

Author	Year	a/d	d_e*	H_w**	b_w***	ρ_f%****	Fiber type	ρ_v%*****	Shear capacity
		-	mm	mm	Mm	-	-	-	kN
[92]	2005	3.0	600	400	50	0–2.5	S&H	0.0	330–497
[93]	2018	3.6	320	140	60	0–2.0	S	0.0–2.1	51–578
[24]	2010	2.5	305	140	65	2.0–2.5	S	0–0.6	441–638
[26]	2013	1.8	305	240	150	0.9–1.0	S	0–0.25	1136–1818
[27]	2019	4.4	305	130	50	0.0	-	0.0	38
[94]	2008	3.8	317.5	160	60	2.5	S	0.0	134–293
[29]	2010	2.3	763	442	99	1.5–2.5	S	0–0.8	1880–2140
[30]	2013	1.8–4.5	620	450	50	1.0–1.5	S	0.0	330–582
[31]	2012	2.5–3.4	645	400	50	1.0–2.0	S	0.0	297–614
[95]	2017	2.0	305	140	65	0–2.5	S	0–0.1	181–630
[33]	2008	4–8	397	230	50	1.0–3.0	S	0.0	220–600
[96]	2004	5.1	240	150	70	2.5	S	0.0	273
[97]	2005	2.0–2.5	810	381	148	2.0	S	0.0	2200–3450
[13]	2022	1.5–2.5	790–1374	148–660	76	0.0–2.0	S	0.0–1.7	1279–2258
[35]	2022	3.5	826–1029	406–610	76–102	2.0	S	0.0–5.2	1236–1491
[36]	2022	1.1–3.2	1029	370	70	2.0	S	1.6	1622–2800
[37]	2019	3.17	1029	105	40	0.5–2.0	S	0.0–0.74	52–97
[39]	2019	1.8–2.6	183	225	150	1.0–2.0	S	0.1–0.3	104–186
[40]	2019	1.5–3.3	260	350	165	0.0–2.25	S&H	0.0	104–674
[41]	2019	1.5–3.5	200	250	150	1.0–3.0	S	0–0.6	250–774
[42]	2018	2.5–4	112	140	100	0.0–2.0	S	0.0	36–125
[43]	2013	2.0	130	150	100	0.0–2.0	S	0.0	18–30
[44]	2016	3.0	240	290	150	1.5	S	0–0.9	172–441
[45]	2018	1.2	125	152	152	2.0	S	0.0	332–476
[46]	2019	4.0	124	150	100	0.0–1.5	S	0.0	36–72
[98]	2022	1.5–3.3	280	350	165	0.0–1.5	H	0.0	77–678
[48]	2022	1.5–3.0	350	350	250	2.7	S	0.0	608–1293
[49]	2022	0.9	525	600	150	0.0–3.0	S	0–0.4	609–1392.2
[50]	2021	2.0–3.4	280	350	200	0.0–2.0	S	0–0.5	111–347
[51]	2018	0.8–0.9	350	350	80	1.5	H	0.5–1.7	415–530
[99]	2019	2.0	350	350	70	0.8	S	0.0	224–316
[52]	2020	1.3	223	60	50	1.5–2.5	S	0.0	140–198
[53]	2019	1.1–3.0	250	170	50	1.6	S	0.6–1.3	249–378
[54]	2022	1.2–2.1	700	800	200	2.0	S	0.0–0.5	3075–4461
[55]	2022	1.6–2.6	450	320	100	2.0	S	0.0–0.7	222–488
[56]	2021	2.0–3.0	255	240	140	0.0–1.5	S	0.0	163–248
[57]	2017	1.8–2.6	183	225	150	1.0–2.0	S	0.3	104–186
[58]	2020	1.5–2.3	200	250	150	1.0–3.0	S	0.0–0.8	301–651
[59]	2023	1.0–1.5	270	260	50	1.0–2.0	S	0.0–0.8	317–590
[60]	2023	1.2–1.6	250	300	150	1.0–3.0	S	0.0–0.4	445–720
[61]	2023	1.7–2.9	160	100	60	1.0–2.0	S-PE	0.0–0.4	255–441
[62]	2015	5.2–5.4	265	150	70	1.0	S	0.0	364–366
[63]	2017	2.5–3.5	445–625	250	40	1.5	S	0.0	340–446
[64]	2019	2.8–3.5	512–913	290–678	40–50	1.0–2.0	S	0.0–0.5	380–1083
[65]	2010	2.8	180	120	20	0.0–1.0	S	0.0–0.1	92–115
[66]	2022	1.5–2.5	320	320	200	1.0–2.0	S	0.0	646–991
[67]	2024	1.6	450	270	65	0.0–2.0	S&H	0.0	607–919
[68]	2020	1.5–3.3	260	300–350	150	0.0–1.5	H	0.0	60–363
[69]	2023	1.2–3.1	245	300	200	1.0–2.0	S	0.0	292–1487
[70]	2024	1.3–2.8	291–345	715	100	2.0	S	0.0	1864–3203

*de: effective depth
* *H_w: height of the web
* ** b_w: width of the web
* ** *ρ_f%: fiber reinforcement ratio
* ** ** ρ_v%: transverse reinforcement ratio

5. Discussion of model predictions

An evaluation for the accuracy of the proposed model compared to the actual results for shear-critical UHPC beams spanning was conducted spanning a wide range of parameters, the specific ranges of these parameters are detailed in Table A.2 in the appendix. The analysis compared the model's performance across different cross-sectional shapes, including rectangular, I-sections, composite sections, T-sections, hollow-box sections, and optimized sections of varying widths, as illustrated in Fig. 17. The comparison results, along with an overview of performance indicators, are presented in Table 5.

The model performed reasonably well in calculating the capacity of the shear-critical I-section and optimized section beams. While the model exhibited reduced accuracy when calculating the capacity of T-section beams, it should be noted that only 6 out of the 311 beams in the database were T-sections. As such, the variability in these results is to be expected given the limited data available for this beam type.

Additionally, the model was assessed for its performance in predicting the behavior of with conventional shear reinforcement, as shown in Fig. 19. The results indicate that the model can accurately calculate the shear capacity of transversely reinforced shear-critical UHPC beams with an R^2 equal to 0.96, and an average calculated-to-experimental results ratio of 1.01, and a coefficient of variation (COV) equal to 0.21. This suggests that the model's assumption regarding transverse reinforcement yielding at the ultimate shear capacity of UHPC beams is valid.

6. Conclusions

This study introduces a hybrid model for evaluating the shear strength of UHPC members. The following conclusions can be made:

1. The MCFT formulation is a valid platform for developing a shear strength model suited for UHPC members. The defining characteristic of the approach presented in this paper lies the integration of the MCFT theoretical formulations with elements derived from experimental observations and analytical studies to account for the implications of cross-sectional shape effect and the fiber orientation.
2. Utilizing a previously developed ML model for characterizing the uniaxial direct tension behavior of UHPC was crucial for verifying the accuracy of the shear strength model proposed in this paper. This necessity arose because many experimental studies did not characterize the direct tension behavior of the UHPC mix used in the beams tested.
3. The analysis of failure modes at different effective depths shows that the presence of fiber reinforcement in shear-critical UHPC beams minimizes the size effect.
4. The proposed hybrid model proved to be an effective tool in predicting the shear strength of UHPC members. An indication of the accuracy of the model consists of the coefficient of determination R^2 of 0.95, average actual-to-predicted strength equal to 1.05, and a coefficient of variation of 0.27.
5. The model demonstrated reliable results in calculating the shear strength of shear-critical UHPC members with various cross-sectional shapes, including rectangular, I-sections, T-sections, hollow-box sections, and optimized sections. This accuracy is attributed to the inclusion of the shape effect in the model.
6. The model had reasonable accuracy in estimating the shear strength of transversely reinforced shear-critical UHPC beams across various transverse reinforcement ratios.

CRediT authorship contribution statement

Anca Ferche: Writing – review & editing, Supervision, Project administration, Investigation. **Amjad Diab:** Writing – original draft, Methodology, Investigation.

Declaration of Competing Interest

The authors declare that they have no known competing financial interests or personal relationships that could have appeared to influence the work reported in this paper.

Acknowledgment

The authors would like to acknowledge the Daniel P. Jenny Research Fellowship program of the Precast/Prestressed Concrete Institute (PCI) for providing funding for this research.

Appendix A

Fig A.1
Table A.2

Data availability

Data available in online repository. The database link is provided in the paper

References

[1] V.H. Perry, P.J. Seibert, Fifteen Years of UHPC Construction Experience in Precast Bridges in North America, in: RILEM-Fib-AFGC Int. Symposium on Ultra-High Performance Fibre-Reinforced Concrete, RILEM, Marseille, 2013.
[2] A. Akhnoukh, P. Skinner, The Future of Ultra-High-Performance Concrete in Infrastructure Projects in the United States, in: A Pathway to Safe, Smart, and Resilient Road and Mobility Networks, 2024: pp. 73–77. ⟨https://doi.org/10.1007/978-3-031-47612-9_8⟩.
[3] Ding Y, Zeng B, Zhou Z, Wei Y, Huang Y. Behavior of UHPC columns confined by high-strength transverse reinforcement under eccentric compression. J Build Eng 2023;70:106352. https://doi.org/10.1016/j.jobe.2023.106352.
[4] Zhang R, Hu P, Chen K, Li X, Yang X. Flexural behavior of T-shaped UHPC beams with varying longitudinal reinforcement ratios. Materials 2021;14:5706. https://doi.org/10.3390/ma14195706.
[5] Kodsy A, Morcous G. Shear strength of ultra-high-performance concrete (UHPC) beams without transverse reinforcement: prediction models and test data. Materials 2022;15:4794. https://doi.org/10.3390/ma15144794.
[6] Wang Q, Song H-L, Lu C-L, Jin L-Z. Shear performance of reinforced ultra-high performance concrete rectangular section beams. Structures 2020;27:1184–94. https://doi.org/10.1016/j.istruc.2020.07.036.
[7] Ding Y, Zhou Z, Wei Y, Huang Y, Tian H. Axial compressive behavior of ultra-high performance concrete confined by high-strength transverse reinforcements. Constr Build Mater 2022;324:126518. https://doi.org/10.1016/j.conbuildmat.2022.126518.
[8] Dogu M, Menkulasi F. A flexural design methodology for UHPC beams posttensioned with unbonded tendons. Eng Struct 2020;207:110193. https://doi.org/10.1016/j.engstruct.2020.110193.
[9] Yao Y, Mobasher B, Wang J, Xu Q. Analytical approach for the design of flexural elements made of reinforced <scp>ultra-high< /scp> performance concrete. Struct Concr 2021;22:298–317. https://doi.org/10.1002/suco.201900404.
[10] El-Helou RG, Graybeal BA. Flexural behavior and design of ultrahigh-performance concrete beams. J Struct Eng 2022;148. https://doi.org/10.1061/(ASCE)ST.1943-541X.0003246.
[11] fib, fib Model Code for Concrete Structures, International Federation for Structural Concrete, Lausanne, Switzerland, 2020.
[12] AFGC (Association Francaise de Génie Civil), Ultra High Performance Fibre-Reinforced Concretes, Recommendations, Paris, France, 2013.
[13] M. Tadros, J. Lawler, M. El-Khier, D. Gee, A. Kurt, G. Lucier, E. Wagner, Implementation of Ultra-High Performance Concrete in Long-Span Precast Pretensioned Elements for Concrete Buildings and Bridges, 2021.
[14] AASHTO LRFD Guide Specifications for Highway Bridge Design with Ultra-High Performance Concrete, 2024.
[15] Vecchio FJ, Collins MP. The modified compression-field theory for reinforced concrete elements subjected to shear. Acids Struct J 1986;83.
[16] AASHTO LRFD bridge design specifications, Washington, 2020.
[17] CSA Group, CSA S6-19. Canadian highway bridge design code, Toronto, Ontario, 2019.
[18] Ross B, Tarawneh A, Naser M, Ferche A, Diab A. Comparison of recent shear capacity models against experimental and simulation databases of prestressed UHPC beams. PCI J 2024.
[19] Metje K, Leutbecher T. Verification of the shear resistance of UHPFRC beams – Design method for the German DAfStb Guideline and database evaluation. Eng Struct 2023;277:115439. https://doi.org/10.1016/j.engstruct.2022.115439.
[20] Diab A, Ferche A. Prediction of the tensile properties of UHPC using artificial neural network. Acids Struct J 2023;121. https://doi.org/10.14359/51740245.
[21] A. Diab, A. Ferche, UHPC beams database, ⟨Https://Www.Kaggle.Com/Dsv/8422136⟩ (2024).
[22] Voo JYL. An investigation into the behaviour of prestressed reactive powder concrete girders subject to non-flexural actions. UNSW 2004.
[23] Mészöly T, Randl N. Shear behavior of fiber-reinforced ultra-high performance concrete beams. Eng Struct 2018;168:119–27. https://doi.org/10.1016/j.engstruct.2018.04.075.
[24] Baby F, Marchand P, Toutlemonde F. Shear behavior of ultrahigh performance fiber-reinforced concrete beams. I: experimental investigation. J Struct Eng 2014;140. https://doi.org/10.1061/(asce)st.1943-541x.0000907.
[25] Zagon R, Matthys S, Kiss Z. Shear behaviour of SFR-UHPC I-shaped beams. Constr Build Mater 2016;124:258–68. https://doi.org/10.1016/j.conbuildmat.2016.07.075.
[26] A. Ali, Behaviour of Prestressed Ultra-High Performance Concrete I-Beams Subjected to Shear and Flexure, 2013.
[27] Hasgul U, Yavas A, Birol T, Turker K. Steel fiber use as shear reinforcement on I-shaped UHP-FRC beams. Appl Sci 2019;9. https://doi.org/10.3390/app9245526.
[28] J. Hegger, G. Bertram, Shear carrying capacity of Ultra-High Performance Concrete beams, (2008).
[29] C.K. Crane, SHEAR AND SHEAR FRICTION OF ULTRA-HIGH PERFORMANCE CONCRETE BRIDGE GIRDERS A Dissertation Presented to The Academic Faculty, 2010.
[30] Voo YL, Foster SJ, Voo CC. Ultrahigh-performance concrete segmental bridge technology: toward sustainable bridge construction. J Bridge Eng 2015;20. https://doi.org/10.1061/(asce)be.1943-5592.0000704.
[31] Yang IH, Joh C, Kim BS. Shear behaviour of ultra-highperformance fibre-reinforced concrete beams without stirrups. Mag Concr Res 2012;64:979–93. https://doi.org/10.1680/macr.11.00153.

[32] Baby F, Marchand P, Toutlemonde F. Shear behavior of ultrahigh performance fiber-reinforced concrete beams. I: Experimental investigation. J Struct Eng 2014;140. https://doi.org/10.1061/(ASCE)ST.1943-541X.0000907.
[33] X. Wu, S.-M. Han, First Diagonal Cracking and Ultimate Shear of I-Shaped Reinforced Girders of Ultra High Performance Fiber Reinforced Concrete without Stirrup, 2009.
[34] B. Graybeal, Structural Behavior of Ultra-High Performance Concrete Prestressed I-Girders, 2006.
[35] El-Helou RG, Graybeal BA. Shear behavior of ultrahigh-performance concrete pretensioned bridge girders. J Struct Eng 2022;148. https://doi.org/10.1061/(asce)st.1943-541x.0003279.
[36] Feng W, Feng H, Zhou Z, Shi X. Analysis of the shear capacity of ultrahigh performance concrete beams based on the modified compression field theory. Adv Mater Sci Eng 2021;2021. https://doi.org/10.1155/2021/5569733.
[37] Qi J, Ding X, Wang Z, Hu Y. Shear strength of fiber-reinforced high-strength steel ultra-high-performance concrete beams based on refined calculation of compression zone depth considering concrete tension. Adv Struct Eng 2019;22:2006–18. https://doi.org/10.1177/1369433219829805.
[38] Preinstorfer P, Huber P, Huber T, Kromoser B, Kollegger J. Experimental investigation and analytical modelling of shear strength of thin walled textile-reinforced UHPC beams. Eng Struct 2021;231:111735. https://doi.org/10.1016/j.engstruct.2020.111735.
[39] Ahmad S, Bahij S, Al-Osta MA, Adekunle SK, Al-Dulaijan SU. Shear behavior of ultra-high-performance concrete beams reinforced with high-strength steel bars. Acids Struct J 2019;116:3–14. https://doi.org/10.14359/51714484.
[40] M. Bermudez, C.-C. Hung, Shear Behavior of Ultra High Performance Hybrid Fiber Reinforced Concrete Beams Shear Behavior of Ultra-High Performance Hybrid Fiber Reinforced Concrete Beams, n.d.
[41] Cao X, Fu F, Deng XF, Qian K, Jin LZ. Shear capacity of reactive powder concrete beams using high-strength steel reinforcement. Proc Inst Civ Eng: Struct Build 2021;174:276–91. https://doi.org/10.1680/jstbu.19.00051.
[42] Ridha MMS, Sarsam KF, Al-Shaarbaf IAS. Experimental study and shear strength prediction for reactive powder concrete beams. Case Stud Constr Mater 2018;8:434–46. https://doi.org/10.1016/j.cscm.2018.03.002.
[43] Kamal MM, Safan MA, Etman ZA, Salama RA. Behavior and strength of beams cast with ultra high strength concrete containing different types of fibers. HBRC J 2014;10:55–63. https://doi.org/10.1016/j.hbrcj.2013.09.008.
[44] Lim WY, Hong SG. Shear tests for ultra-high performance fiber reinforced concrete (UHPFRC) beams with shear reinforcement. Int J Concr Struct Mater 2016;10:177–88. https://doi.org/10.1007/s40069-016-0145-8.
[45] Pourbaba M, Joghataie A, Mirmiran A. Shear behavior of ultra-high performance concrete. Constr Build Mater 2018;183:554–64. https://doi.org/10.1016/j.conbuildmat.2018.06.117.
[46] Yavaş A, Hasgul U, Turker K, Birol T. Effective fiber type investigation on the shear behavior of ultrahigh-performance fiber-reinforced concrete beams. Adv Struct Eng 2019;22:1591–605. https://doi.org/10.1177/1369433218820788.
[47] Bermudez M, Wen K-W, Hung C-C. A comparative study on the shear behavior of UHPC beams with macro hooked-end steel fibers and PVA fibers. Materials 2022;15:1485. https://doi.org/10.3390/ma15041485.
[48] Yang J, Doh JH, Yan K, Zhang X. Experimental investigation and prediction of shear capacity for UHPC beams. Case Stud Constr Mater 2022;16. https://doi.org/10.1016/j.cscm.2022.e01097.
[49] Chen B, Zhou J, Zhang D, Su J, Nuti C, Sennah K. Experimental study on shear performances of ultra-high performance concrete deep beams. Structures 2022;39:310–22. https://doi.org/10.1016/j.istruc.2022.03.019.
[50] il Bae B, Lee MS, Choi CS, Jung HS, Choi HK. Evaluation of the ultimate strength of the ultra-high-performance fiber-reinforced concrete beams. Appl Sci 2021;11. https://doi.org/10.3390/app11072951.
[51] Yousef AM, Tahwia AM, Marami NA. Minimum shear reinforcement for ultra-high performance fiber reinforced concrete deep beams. Constr Build Mater 2018;184:177–85. https://doi.org/10.1016/j.conbuildmat.2018.06.022.
[52] Ţibea C, Bompa D v. Ultimate shear response of ultra-high-performance steel fibre-reinforced concrete elements. Arch Civ Mech Eng 2020;20. https://doi.org/10.1007/s43452-020-00051-z.
[53] Zheng H, Fang Z, Chen B. Experimental study on shear behavior of prestressed reactive powder concrete I-girders. Front Struct Civ Eng 2019;13:618–27. https://doi.org/10.1007/s11709-018-0500-8.
[54] Zhou L, Wan S. Shear behavior of UHPC beams with small shear span to depth ratios based on MSTM. Case Stud Constr Mater 2022;16. https://doi.org/10.1016/j.cscm.2022.e01134.
[55] Cao X, He D, Qian K, Fu F, Deng XF, Wang L. Shear behavior of glass FRP bars-reinforced ultra-high performance concrete I-shaped beams. Struct Concr 2022. https://doi.org/10.1002/suco.202100801.
[56] Jabbar AM, Hamood MJ, Mohammed DH. The effect of using basalt fibers compared to steel fibers on the shear behavior of ultra-high performance concrete T-beam. Case Stud Constr Mater 2021;15. https://doi.org/10.1016/j.cscm.2021.e00702.
[57] Bahij S, Adekunle SK, Al-Osta M, Ahmad S, Al-Dulaijan SU, Rahman MK. Numerical investigation of the shear behavior of reinforced ultra-high-performance concrete beams. Struct Concr 2018;19:305–17. https://doi.org/10.1002/suco.201700062.
[58] Wang Q, Song HL, Lu CL, Jin LZ. Shear performance of reinforced ultra-high performance concrete rectangular section beams. Structures 2020;27:1184–94. https://doi.org/10.1016/j.istruc.2020.07.036.
[59] Feng J, Li P, Wu J, Jiang H, Tian Y, Sun X. Shear behavior of externally prestressed UHPC beams without stirrups. Case Stud Constr Mater 2023;18. https://doi.org/10.1016/j.cscm.2022.e01766.
[60] Chen B, Zhou J, Zhang D, Sennah K, Nuti C. Shear performances of reinforced ultra-high performance concrete short beams. Eng Struct 2023;277:115407. https://doi.org/10.1016/j.engstruct.2022.115407.
[61] Zeng JJ, Pan BZ, Fan TH, Zhuge Y, Liu F, Li LJ. Shear behavior of FRP-UHPC tubular beams. Compos Struct 2023;307. https://doi.org/10.1016/j.compstruct.2022.116576.
[62] Lee J-H, Hong S-G. Shear strength of ultra-high performance fiber-reinforced concrete(UHPFRC) I-shaped beams without stirrup. J Korea Concr Inst 2017;29:53–64. https://doi.org/10.4334/jkci.2017.29.1.053.
[63] Schramm N, Fischer O. Querkraftversuche an profilierten Spannbetonträgern aus UHPFRC. Beton- Und Stahlbetonbau 2019;114:641–52. https://doi.org/10.1002/best.201900022.
[64] K. Telleen, T. Noshiravani, R. Galrito, E. Brühwiler, Experimental investigation into the shear resistance of a reinforced UHPFRC web element, n.d.
[65] Ma K, Ma Y, Liu B. Experimental investigation on ultra high performance fiber reinforced concrete beams. Mech Adv Mater Struct 2023;30:1155–71. https://doi.org/10.1080/15376494.2022.2028947.
[66] Lakavath C, Prakash SS. Influence of fiber dosage, fiber type, and level of prestressing on the shear behaviour of UHPFRC I-girders. Eng Struct 2024;300:117146. https://doi.org/10.1016/j.engstruct.2023.117146.
[67] Hung C., Wen K.Investigation of shear strength of ultra-high performance concrete beams without stirrup, in: The 17th World Conference on Earthquake Engineering, 2020..
[68] Li P, Cheng Q, Chen N, Tian Y, Fang J, Jiang H. Experimental study on shear behavior of non-stirrup ultra-high performance concrete beams. Materials 2023;16:4177. https://doi.org/10.3390/ma16114177.
[69] Zhang L, Den B, He B, Jiang H, Xiao J, Tian Y, Fang J. Experimental investigation on shear behavior of non-stirrup uhpc beams under larger shear span-depth ratios. Prepr Org 2024.
[70] Tu W, Cheng Q, Zhang L, Li P, Jiang H, Tian Y, Fang J. Shear performance of 25 m full-scale prestressed UHPC-NC composite I-beam without stirrups. Case Stud Constr Mater 2024;21:e03942. https://doi.org/10.1016/j.cscm.2024.e03942.
[71] Zhang L, Deng B, He B, Jiang H, Xiao J, Tian Y, Fang J. Experimental investigation on shear behavior of non-stirrup UHPC beams under larger shear span–depth ratios. Buildings 2024;14:1374. https://doi.org/10.3390/buildings14051374.
[72] Yang J, Doh J-H, Yan K, Zhang X. Experimental investigation and prediction of shear capacity for UHPC beams. Case Stud Constr Mater 2022;16:e01097. https://doi.org/10.1016/j.cscm.2022.e01097.
[73] Graybeal B, Marshall D. Cylinder or Cube: Strength Testing of 80 to 200 MPa (11.6 to 29 ksi) Ultra-High-Performance Fiber-Reinforced Concrete. ACI Mater J; 2008. p. 603–9.
[74] Abellán-García J. Four-layer perceptron approach for strength prediction of UHPC. Constr Build Mater 2020;256:119465. https://doi.org/10.1016/j.conbuildmat.2020.119465.
[75] El-Helou RG, Graybeal BA. Shear behavior of ultrahigh-performance concrete pretensioned bridge girders. J Struct Eng 2022;148. https://doi.org/10.1061/(asce)st.1943-541x.0003279.
[76] Nawy E. Prestressed Concrete: A Fundamental Approach. Pearson; 2009.
[77] Ghafari E, Ghahari SA, Costa H, Júlio E, Portugal A, Durães L. Effect of supplementary cementitious materials on autogenous shrinkage of ultra-high performance concrete. Constr Build Mater 2016;127:43–8. https://doi.org/10.1016/j.conbuildmat.2016.09.123.
[78] Collins MP, Mitchell D. Prestressed Concrete Structures. Response Publications; 1997.
[79] E.C. Bentz, F.J. Vecchio, M.P. Collins, Simplified Modified Compression Field Theory for Calculating Shear Strength of Reinforced Concrete Elements, ACI Structural Journal (20016) 614–624.
[80] El-Helou RG, Graybeal BA. Shear design of strain-hardening fiber-reinforced concrete beams. J Struct Eng 2023;149. https://doi.org/10.1061/jsendh.steng-11065.
[81] Diab A, Ferche A. Modeling the Response of UHPC Shear-Critical Beams: Integrating Nonlinear Finite Element Analysis and Machine Learning. SSRN; 2024.
[82] Huang H, Su A, Gao X, Yang Y. Influence of formwork wall effect on fiber orientation of UHPC with two casting methods. Constr Build Mater 2019;215:310–20. https://doi.org/10.1016/j.conbuildmat.2019.04.200.
[83] Martinie L, Roussel N. Simple tools for fiber orientation prediction in industrial practice. Cem Concr Res 2011;41:993–1000. https://doi.org/10.1016/j.cemconres.2011.05.008.
[84] Huang H, Gao X, Li L, Wang H. Improvement effect of steel fiber orientation control on mechanical performance of UHPC. Constr Build Mater 2018;188:709–21. https://doi.org/10.1016/j.conbuildmat.2018.08.146.
[85] Huang H, Gao X, Teng L. Fiber alignment and its effect on mechanical properties of UHPC: An overview. Constr Build Mater 2021;296:123741. https://doi.org/10.1016/j.conbuildmat.2021.123741.
[86] B. Yap, Behaviour of Ultra High Performance Fibre Reinforced Concrete Subjected to Pure Shear, 2020. ⟨http://ezproxy.lib.utexas.edu/login?url=https://www.proquest.com/dissertations-theses/behaviour-ultra-high-performance-fibre-reinforced/docview/2425651578/se-2?accountid= 7118⟩.
[87] El-Helou RG, Graybeal BA. Shear behavior of ultrahigh-performance concrete pretensioned bridge girders. J Struct Eng 2022;148. https://doi.org/10.1061/(ASCE)ST.1943-541X.0003279.
[88] C. Crane, Shear and shear friction of ultra-high performance concrete bridge girders, Georgia Institute of Technology, 2010..

[89] Foster SJ, Bentz E. Design of prestressed girders for shear. Struct Concr 2024;25: 780–95. https://doi.org/10.1002/suco.202300738.
[90] Liu R-R, Ding R, Fan J-S, Tao M-X. Constitutive laws of softened UHPC in biaxial tension–compression: experimental study using a planar bi-directional element tester. Constr Build Mater 2023;401:132966. https://doi.org/10.1016/j.conbuildmat.2023.132966.
[91] Collins MP, Mitchell D, Adebar P, Vecchio F. A general shear design method. Acids Struct J 1996;93:36–60.
[92] Voo YL, Foster SJ, Gilbert RI. Shear strength of fiber reinforced reactive powder concrete prestressed girders without stirrups. J Adv Concr Technol 2006;4:123–32. https://doi.org/10.3151/jact.4.123.
[93] Mészöly T, Randl N. Shear behavior of fiber-reinforced ultra-high performance concrete beams. Eng Struct 2018;168:119–27. https://doi.org/10.1016/j.engstruct.2018.04.075.
[94] Hegger J, Bertram G. Shear carrying capacity of ultra-high performance concrete beams. Tailor Made Concr Struct 2008:341. 7., (n.d.).
[95] Baby F, Billo J, Renaud JC, Massotte C, Marchand P, Toutlemonde F. Ultimate shear strength of ultra high performance fibre-reinforced concrete beams. HIPERMAT 2012;2012:485–92 (n.d.).
[96] Hegger J., Tuchlinski D., Kommer B.(2004, September). Bond anchorage behavior and shear capacity of ultra high performance concrete beams. In Proceedings of the International Symposium on Ultra High Performance Concrete (pp. 351-360)., (n. d.)..
[97] T. Fairbank Highway Research Center, Structural Behavior of Ultra-High Performance Concrete Prestressed I-Girders, 2006.
[98] Bermudez M, Wen KW, Hung CC. A comparative study on the shear behavior of UHPC beams with macro hooked-end steel fibers and PVA fibers. Materials 2022; 15(4):1485 (n.d.).
[99] Fu J, Wang ZS, Min YB, Ding QJ. Research on shrinkage control technology of lightweight ultra-high performance concrete. In Green and Intelligent Technologies for Sustainable and Smart Asphalt Pavements. CRC Press; 2021. p. 38–43 (n.d.).

Amjad Diab is a Ph.D. student at the Maseeh Department of Civil, Architectural and Environmental Engineering, The University of Texas at Austin. His research interests include performance assessment and analysis of concrete structures, structural implications of deterioration mechanisms, and sustainability of concrete structures.

Anca Ferche is an Assistant Professor in the Maseeh Department of Civil, Architectural and Environmental Engineering, The University of Texas at Austin, TX. Her research interests include performance assessment and analysis of reinforced concrete structures, concrete deterioration mechanisms, and rehabilitation of structures.